# A Real-time Strontium-90 Counter

Hiroshi Ito, Hideyuki Kawai, Satoshi Kodama and Makoto Tabata

***Abstract*—A new type of detector, a real-time strontium-90 ($^{90}$Sr) counter, is developed that is sensitive to $^{90}$Sr but less so to caesium-137 ($^{137}$Cs), potassium-40 ($^{40}$K), and cosmic rays. The detector is based on a threshold-type Cherenkov counter using silica aerogel with a refractive index of less than 1.042 and a plastic scintillation detector covering the Cherenkov counter to suppress cosmic-ray events. Because the threshold energy is set to $1.31\ \mathrm{MeV}$ in the Cherenkov counter, the beta rays from $^{90}$Y can be identified in the radiation environmental. In the 2011 Fukushima Nuclear Accident in Japan, fisheries in particular were severely damaged by radioactive contamination. Recent studies of the contaminated waters have focused on radiation with longer half-lives, in particular $^{90}$Sr and $^{137}$Cs, and so the detector performance was evaluated using these radioactive sources. As a result, the absolute efficiencies of $^{90}$Sr, $^{137}$Cs, and $^{40}$K at the center of the effective area of the detector were evaluated to be $[1.79 \pm 0.04\ (\mathrm{stat}) \pm 0.36\ (\mathrm{sys}) \times 10^{-3}$, $[1.32 \pm 0.19\ \ (\mathrm{stat}) \pm 0.014\ \ (\mathrm{sys})] \times 10^{-6}$, and $[5.77 \pm 7.83\ (\mathrm{stat}) \pm 0.02\ (\mathrm{sys})] \times 10^{-6}\ \mathrm{Bq^{-1}\ s^{-1}}$, respectively. The response linearity was observed in the relationship between the radioactivity and count rate. Thus, the detector could measure the radioactivity concentration of $^{90}$Sr in the sample. By using these results, the detection limits of the concentrations of $^{90}$Sr in seawater and seafood samples could be established.**

***Index Terms*—Beta-ray Detectors, Cherenkov Detectors, Radiation Environment, Strontium-90**

## I. Introduction

THE Great East Japan Earthquake in March, 2011 caused a major accident at the Fukushima Daiichi Nuclear Power Plant that resulted in radionuclides being spread over Japan and the Pacific Ocean. After the earthquake disabled the radiation dose monitoring centers located near the reactor, weather simulations by Katata et al. were used to determine that the major spread of isotopes was northwest from the reactor toward the village of Iitate [1]. On April 10, 2011, K. Shozugawa et al. collected samples of soil, plants, and water from Iitate village and measured radionuclides such as iodine-131 ($^{131}$I), caesium-134 ($^{134}$Cs), and caesium-137 ($^{137}$Cs) in the samples using a Ge(Li) semiconductor detector [2]. In the immediate aftermath of the nuclear accident, most studies were focused on internal radiation exposure of the thyroid to $^{131}$I, which has a relatively short radioactive half-life. Most recent studies have focused on internal exposure to $^{90}$Sr and $^{137}$Cs, which have longer half-lives.

Recently, fisheries activity has ceased around Fukushima because of the radionuclides that have entered the Pacific Ocean around. The Federation of Fisheries Cooperative Associations of Fukushima Prefecture built a system for monitoring the concentration of contamination in seafood. This has measured radioactivity associated with of $^{134}$Cs and $^{137}$Cs (the letter being commonly known as radiocaesium) in individual samples of fish and seafood by using a NaI(Tl) scintillation detector. Although the results as reported are below the accepted limit of contamination in food of $100\ \mathrm{Bq\ kg^{-1}}$ (as set by the Ministry of Health, Labour and Welfare, Japan), fishing activities are yet to recommence because the absence of strontium-90 ($^{90}$Sr) in food cannot be certified. Strontium-90 is more dangerous than $^{137}$Cs and its concentration is difficult to measure in fish and seafood.

Caesium is an alkali metal (similar to sodium) that is excreted with a biological half-life of $70\ \mathrm{d}$ if it enters the body, whereas strontium is an alkali earth metal (similar to calcium) that accumulates in the bone. According to the International Commission on Radiological Protection (ICRP), the effective dose coefficients of $^{90}$Sr ($^{90}$Y) and $^{137}$Cs for adults are $2.4 \times 10^{-8}$ and $4.6 \times 10^{-9}\ \mathrm{Sv\ Bq^{-1}}$, respectively. Although the $^{90}$Sr and $^{137}$Cs ratio of these coefficients is approximately 5 for a whole-body dose, it is important to compare the dose coefficients in different tissues. In red marrow, the dose coefficients of $^{90}$Sr and $^{137}$Cs are estimated as $1.6 \times 10^{-7}$ and $4.4 \times 10^{-9}\ \mathrm{Sv\ Bq^{-1}}$, respectively, which is a $^{90}$Sr and $^{137}$Cs ratio 36. This ratio rises with decreasing age, reaching an estimated maximum of 126 in infants [3]. Therefore, $^{90}$Sr is more dangerous than $^{137}$Cs for internal exposures.

It is ease to measure the radioactivity of radiocaesium by using gamma-ray spectroscopy. Yamasaki et al. and other researchers measured radiocaesium concentration in estuary sediments from near the Fukushima Daiichi Nuclear Power Plant, and in fish, seafood, and other food from Fukushima Prefecture [4]–[6]. The results of using a chemical extraction method were a $^{90}$Sr concentration of $0.46\ \mathrm{Bq\ kg^{-1}}$ in flatfish and a ratio of $^{90}$Sr/radiocaesium of 0.27 [6]. The conventional method for measuring radioactivity of $^{90}$Sr is based on the chemical extraction of ashed all sample and on measurements of beta rays from pure $^{90}$Y. The necessary time of process time depends on the time interval between the radioactive equilibrium conditions of $^{90}$Sr and $^{90}$Y. Therefore, this method cannot be used to inspect the concentration of $^{90}$Sr in food because the process takes approximately one month [7].

Hence, we have developed a real-time $^{90}$Sr counter that can measure such radioactivity from a sample in an hour without chemical extraction [8], [9]. This detector is sensitive to beta rays from $^{90}$Y but less sensitive to other radiation because

Manuscript received February 21, 2017; This work was supported by (i) JSPS KAKENHI Grant number 25610049, (ii) the Nuclear Safety Institute of Technology via publicly offered research for the Chubu of Electric Power Co., Inc. in 2013, (iii) a special recovery-support program for the Great East Japan Earthquake in 2014, (iv) the New Technology Development Foundation and Venture Business Laboratory, Chiba University, and (v) The Ogasawara Foundation for the Promotion of Science and Engineering in 2016.

H. Ito, H. Kawai, S. Kodama and M. Tabata are with the Graduate of School of Science, Chiba University, Chiba, 268-8522, Japan (e-mails: hiroshi@hepburn.s.chiba-u.ac.jp; kodama@hepburn.s.chiba-u.ac.jp; kawai@hepburn.s.chiba-u.ac.jp; makoto@hepburn.s.chiba-u.ac.jp).

it is based on a threshold-type Cherenkov counter using silica aerogel with a refractive index of less than 1.042. The detection limit of $^{90}$Sr is deteriorated by background events from cosmic rays [9]. Therefore, a veto counter with plastic scintillator plates and wavelength-shifting fibers (WLSFs) was designed and installed over the Cherenkov counter. As such, the detector can be used to measure the radioactivity of $^{90}$Sr in food because 1) it is easy to handle (much like a survey meter), 2) measurements can be made rapidly in an hour, 3) it can be used anywhere outside a radiation controlled area, 4) samples can be prepared without chemical extraction. This paper presents our study of the $^{90}$Sr counter so developed. The detector mechanism and components are described in Section II, performance results are given in Section III, and conclusions are drawn in Section IV.

## II. Real-Time $^{90}$Sr Counter

The detector consists of a trigger counter made of scintillating fibers, an aerogel Cherenkov counter with WLSFs and a veto counter made of plastic scintillators and WLSFs. In this section, the detection mechanism, design of the detector, an electronics, and the logic operation are described in detail.

### A. Detection Mechanism

*1) Cherenkov radiation:* Cherenkov radiation is a form of shock wave. When the speed $v$ of a charged particle is higher than light speed $c/n$ in a material with a refractive index $n$, photons are emitted as Cherenkov radiation. In order to emit Cherenkov photons that are associated only with beta rays from $^{90}$Y in the other radionuclides (e.g., radiocaesium and $^{40}$K), silica aerogel with a refractive index of less than 1.042 was used as the radiator [10], [11]. In this study, silica aerogel with $n = 1.041 \pm 0.001$ and an optical transmission length of $40.8$ mm at a wavelength of 400 nm was installed in the detector [12]. The ratio of the speed of the beta rays to that of light ($\beta = v/c$) is given as

$$\beta = \frac{\sqrt{(m_{\mathrm{e}}c^2 + K)^2 - m_{\mathrm{e}}^2 c^4}}{mc^2 + K}, \tag{1}$$

where $m_{\mathrm{e}}$ is the electron mass and $K$ is the beta-ray kinetic energy. Therefore, the speed ratio of the beta rays with $K = 2.28$ MeV is calculated as $\beta = 0.983$.

The number of emitted photons emitted ($N_{\mathrm{ph}}$) when a beta ray passes through the silica aerogel (with refractive index $n$) is given approximately given as

$$N_{\mathrm{ph}} \sim 2\pi\alpha L \left(1 - \frac{1}{n^2\beta^2}\right) \int \frac{d\lambda}{\lambda^2}, \tag{2}$$

where $\alpha$, $L$, and $\lambda$ are the fine-structure constant, the path length of the beta rays, and the wavelength of the emitted photons, respectively. In the case of the beta rays from the $^{90}$Y in the silica aerogel, the number of photons per unit length is approximately 27.6 cm$^{-1}$ for an integral wavelength range of 300-500 nm considering the absorption spectrum of the WLSFs.

*2) Suppression of background noise from cosmic muons:* The intensity of cosmic muons is known to be approximately $70\ \mathrm{m}^{-2}\ \mathrm{s}^{-1}\ \mathrm{sr}^{-1}$ at ground level. Muons with energies more than a few GeV/$c$ travel at nearly the speed of light because of relativity effects. If muons pass through the silica aerogel, Cherenkov photons are emitted that become background noise. However, such events can be rejected by using the signals from the veto counter that covers the Cherenkov counter.

*3) Suppression of other background noise :* Cherenkov photons are observed using photomultiplier tubes (PMT). Gamma rays from a sample cannot emit Cherenkov photons. However, if gamma rays interact in a photocathode or entrance window of a PMT, noise signals are produced. In the case of gamma rays interacting in the photocathode, the electrons so produced become noise signals by being amplified between the dynodes in the PMT. In contrast, gamma rays that interacted in the entrance window produce electrons that emit photons by satisfying the Cherenkov radiation conditions in the window. Therefore, it is necessary to increase the distance between the PMTs and the sample.

### B. Design of the Detector

The detector design is shown in Fig. 1. The trigger counter is set under the aerogel Cherenkov counter using WLSFs. The entrance window of the detector is $300\ \mathrm{mm} \times 100\ \mathrm{mm}$; nine silica-aerogel tiles and a fiber light guide are used in the Cherenkov counter. The sample must be in the form of a paste that is less than 1-mm thick and that has been dried without chemical extraction. That is because the beta rays emitted from $^{90}$Y can be stopped at a water depth of approximately 10 mm.

*1) Trigger counter:* To satisfy the Cherenkov radiation conditions for beta rays originating from $^{90}$Y, the trigger counter should have minimal energy absorption. The trigger consists of scintillating fibers (type: SCSF-78MJ) manufactured by Kuraray Co., Ltd. [13] and PMTs (type: R9880U-210) produced by Hamamatsu Photonics K. K. [14]; it is wrapped in aluminized Mylar and black vinyl-chloride sheets for light shielding. The fibers have a cross-sectional diameter of a 0.2-mm, a double-cladding structure, and a trapping efficiency of 10.8% by calculated from the total-reflection condition. The PMTs have an 8-mm-diameter photocathode made of ultra-bialkali, and a maximum quantum efficiency of 40% at 400 nm. A sheet with an effective area of $300\ \mathrm{mm} \times 100\ \mathrm{mm}$ is made of scintillating fibers, in which both ends of the fibers are bundled. After polishing, the fiber-end surfaces are connected optically to the PMTs. The detection efficiency of the trigger counter is evaluated as 54.4% using a $^{90}$Sr source, for which the sheet comprised one layer of the fibers to reduce the amount of substance.

*2) Aerogel Cherenkov counter:* To suppress the noise events from gamma rays and to expand the effective area, optical light guides using WLSFs are adopted in the Cherenkov counter. After the Cherenkov photons are absorbed by the WLSFs, the fibers emit photons with longer wavelength. Four PMTs (of

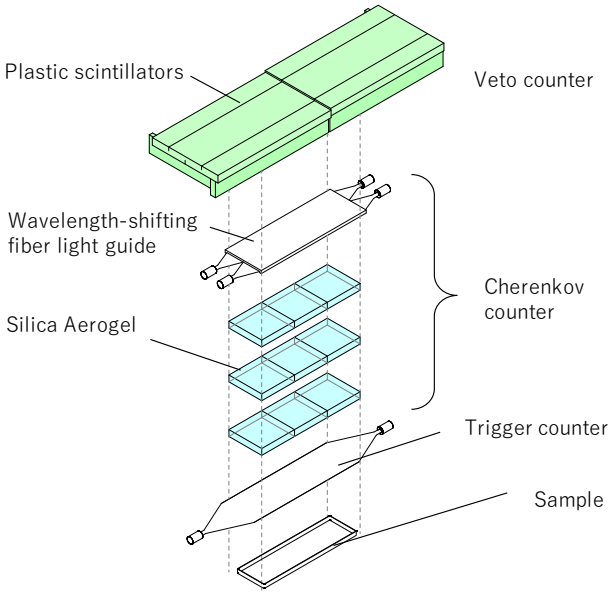


Fig. 1. Detector design. The sample is set under the trigger counter. The entrance window is 300 mm × 100 mm. The Cherenkov counter is placed above the trigger. A total of nine tiles of silica aerogel with a size of 96 mm× 96 mm × 10 mm are used. The veto counter covers these counters in order to detect muons arriving with zenith angles of 0-90°. The wavelength-shifting fibers and PMTs are omitted for the sake of clarity.

the same type as those in the trigger counter) are connected to the both ends of the fibers to observe the red-shifted photons that undergo total internal reflection inside the fibers. The fiber light guides are made of two types of WLSFs—B-3(300)MJ and Y-11(300)MJ, manufactured by Kuraray Co., Ltd.—to extend the range of absorbed wavelengths. The fibers have a cross-sectional diameter of $0.2$ mm, an attenuation length of approximately $1$ m, a double-cladding structure, and a trapping efficiency of $10.8\%$. The shifts of the B-3 and the Y-11are purple-to-blue and blue-to-green, respectively. Because Cherenkov photons cover a continuous spectrum distribution that is inversely proportion to the square of the wavelength (see Eq. (2)), each fiber light guide is made of two layers of the B-3 (upstream) and two layers of the Y-11 (downstream), with the aluminized Mylar reflector being attached downstream of the Y-11. Furthermore, the light guide can absorb any blue photons that leaked from the B-3 into Y-11. The performance of the fiber light guide is evaluated by using cosmic-ray muons. Cherenkov photons are emitted then cosmic muons pass through the silica aerogel, are reflected by the aluminized Mylar, and are observed by the PMTs both directly and via the WLSFs. By comparing the numbers of such photoelectrons, the collection efficiency is evaluated to be approximately $8\%$.

Because the fiber core has a refractive index $n = 1.59$, beta rays with $K > 0.15$ MeV satisfy the Cherenkov condition in the fibers. In the aerogel Cherenkov counter, a silica-aerogel thickness of 29.5 mm or more is required in order violate the Cherenkov condition when the beta rays arrive in the fibers with $K < 1.31$ MeV having passed through the trigger counter. A total of nine ($3 \times 3$) silica-aerogel tiles are used in the Cherenkov counter (see Fig. 1). The size of each of these tiles is 96 mm × 96 mm × 10 mm; thus, the total thickness is 30 mm. In this study, the silica aerogel has two functions as a Cherenkov radiator, and as energy degrader for the beta rays from $^{40}$K.

Beta rays with energies of 1.31-2.28 MeV account for $13.4\%$ of all those emitted from $^{90}$Sr and $^{90}$Y, which is the radiation equilibrium. When those beta rays emitted from $^{90}$Y pass through the silica aerogel (losing energy as they do so), an estimated 14 Cherenkov photons are emitted. The mean number of photoelectrons observed by the PMTs is estimated to be 0.060. This is done by calculating the collection efficiency of the fiber light guides ($8\%$) and the quantum efficiency of the PMTs ($40\%$). The estimation is consistent with experimental value of 0.062. Although the efficiency of the detector results in relatively few photoelectrons, it is important to measure the $^{90}$Sr radioactivity concentration in the sample by identifying the beta rays from $^{90}$Y. The detector can measure this radioactivity concentration with an appropriate measurement time and an absolute efficiency, even for very few photons.

*3) Veto counter:* To suppress background events cause by cosmic-ray muons arriving with zenith angles of 0-90°, a veto counter based on a scintillation detector was designed to cover the trigger and the Cherenkov counters. The veto counter design is shown in Fig. 2. It consists of two units that have plastic scintillators placed on the short, long (two thereof), and top sides, fiber light guides, and a PMT (type: H11934-200). The plastic scintillators used in the study are 5-mm thick and are produced by the Ohyo Koken Kogyo Co., Ltd., Japan.

The unit sizes were determined so that the same number of photoelectrons would be measured when a cosmic muon passed through any of the sides. On the short side, two scintillator plates of 50 mm × 200 mm are connected using EJ-500 optical cement (produced by G-Tech Corp., Japan) to make a single block with a thickness of 10 mm. On each of the two long sides, three plates of 50 mm × 350 mm are connected using the optical cement to make one block with a thickness of 15 mm. On the top side, four plates of 49 mm × 350 mm, two plates of 99 mm × 350 mm, and four plates 100 mm × 350 mm are connected using the optical cement to make one block with a size of 200 mm × 350 mm × 20 mm. This has three grooves with a depth of 10 mm, a width of 1 mm, and a length of 350 mm at the center of the back face and at 50 mm and 150 mm from the edge of the front face.

The light guides, which are four layers of 0.2-mm-diameter Y-11(300)MJ, are connected to both side surfaces of the scintillator blocks and the grooves by using the optical cement. One side of the end of the fibers is connected to the PMT and the other side of the end of the fibers is connected to the aluminized Mylar reflectors. The scintillation photons emitted from these blocks are read by the PMT via the WLSFs.

The two units were assembled to make a scintillation detector with external dimensions of 200 mm × 700 mm × 70 mm and an internal capacity of 170 mm × 680 mm × 50 mm. Wherever cosmic-ray muons pass through the veto counter,

an average of 50–60 photoelectrons are observed, which is deemed to be a sufficient performance.

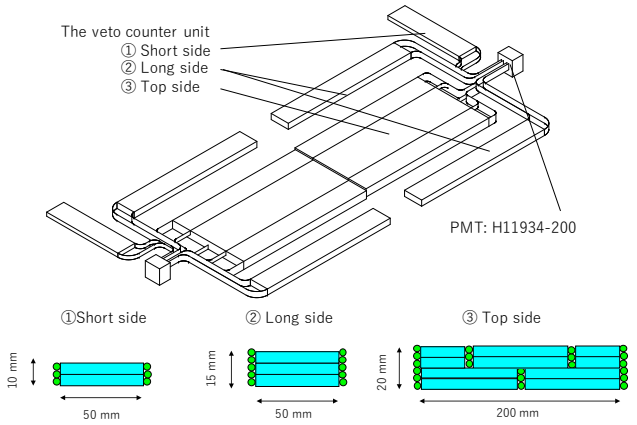


Fig. 2. Veto counter design and sectional views of the scintillator blocks. A single veto counter unit comprises 5-mm-thick, scintillator plates, light guides made of the WLSFs, 0.2-mm-diameter Y-11, and an H11934-200 PMT.

### C. Electronics

An overview of the electronics and pictures of the circuit boards are shown in Fig. 3. The detector is supplied with 100 V of alternating current (AC) voltage from a household power source. After the supplied AC voltage has been converted to a positive 12-V direct current (DC) voltage by an AC–DC converter (HFS50, made by Daitron Co., Ltd., Japan), a DC–DC converter (RP-1637CS made by REPIC Co., Ltd.) supplies DC voltages of $\pm 5$ V and $+12$ V to each HV, and DC voltages of $\pm 5$ V to each DISCR (defined below). The HVs are four-channel high-voltage supply units for PMTs (RP-1637BS, made by REPIC). They each have two high-voltage chips (BP015205n12, made by iseg Spezialelektronik GmbH, Germany), and supply a nominal $1,200$ V to each PMT. The DISCRs are a four-channel discriminators (RP-1637AS, manufactured by REPIC). The threshold voltages are set to 15–25 mV (corresponded to 0.5 p.e.) for the PMTs of the Cherenkov counter and 25–35 mV (corresponded to 1.5 p.e.) for the PMTs of the trigger and the veto counters. The signal cables from the PMTs are connected to the DISCRs. The output from each DISCR are NIM logic signals that are input to a BRoaD NIM logic unit (BRoaD ver. 1, developed by Bee Beans Technologies Co., Ltd.) [15]. In this study, the BRoaD functions as a coincidence module.

### D. Logic Signals

After the pulse signals from the veto-counter PMTs have been discriminated by the DISCR, the 50-ns-wide NIM logic signals are input to the BRoaD. In contrast, the 10-ns-wide NIM signals for the trigger and the Cherenkov counters are delayed by 30 ns before being input to the BRoaD to synchronize with the timing of the veto counter. A schematic time projection of these logic signals is shown in Fig.4. There, $C_j$ is the binary output signal from the discriminator, which $j$ =1–8 is the PMT channel. In order to measure the beta rays from $^{90}$Y, the logic of $Trigger \cdot \overline{VETO} \cdot AC$ is required, where

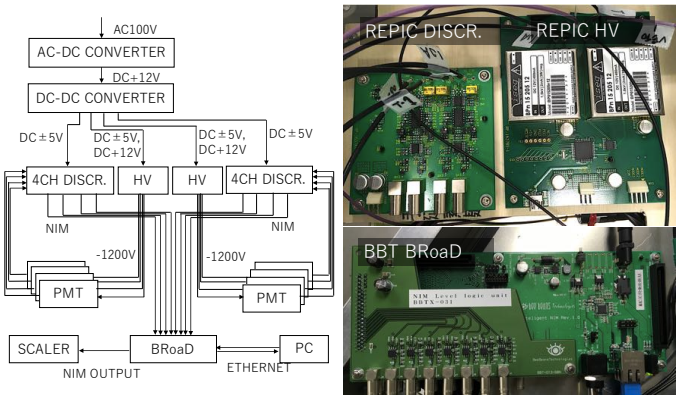


Fig. 3. Overview of the electronics (left); circuit boards (right). DISCR (top center) is an RP-1637AS discriminator, and HV (top right) is an RP-1637BS high-voltage supply for a PMT; both DISCR and HV are made by REPIC Co., Ltd. BRoaD (bottom right) is a NIM logic unit developed by Bee Beans Technologies Co., Ltd.

$Trigger$ is defined as $(C_1 \cdot C_2)$ of the both PMTs connected to the trigger counter, $VETO$ is $(C_3 + C_4)$ of either PMT connected to the veto counter, and $AC$ is a multiplicity logic in the four PMTs connected to the Cherenkov counter. The multiplicity logic is defined as $AC = 1$ when $C_j = 1$ ($j$ = 5–8) ($M$) is greater than a threshold number ($M_{th}$) or $M = M_{th}$. The multiplicity logic represented as $AC(M \geq M_{th})$ and could tune a probability of $^{90}$Sr (as discuss in Section III D.). In order to compare the logic operations for the measurement of $^{90}$Sr, the BRoaD is defined as

$$Trigger \cdot \overline{VETO} \cdot AC(M \geq 1), \quad (3)$$
$$Trigger \cdot \overline{VETO} \cdot AC(M \geq 2), \quad (4)$$
$$Trigger \cdot \overline{VETO}, \quad (5)$$
$$Trigger \cdot AC(M \geq 2). \quad (6)$$

In Eqs. (3) and (4), as the number of threshold ($M_{th}$) increase, the efficiency of detecting $^{90}$Sr is reduced and accidental noise is suppressed. Equation (5) represents the detection of all beta rays in the trigger counter. Equation (6) is the detection based on Cherenkov radiation without the veto counter. By comparing Eqs. (4) and (6), it can be seen that cosmic-ray-muon background events lower the limit for detecting $^{90}$Sr.

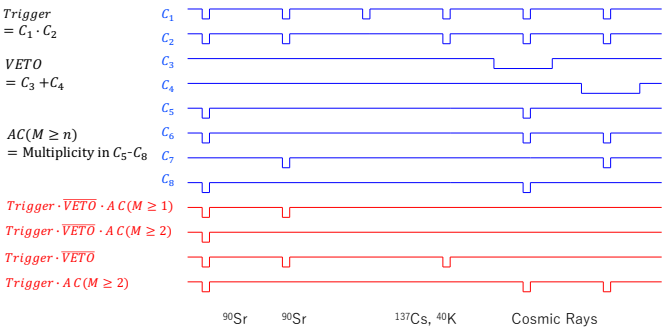


Fig. 4. Time projection of the logic signals. Blue and red lines are NIM signals that are output from the DISCRs and BRoaD, respectively. These logic signals represent the behaviors of $^{90}$Sr, $^{137}$Cs, $^{40}$K, and cosmic-ray muons.

## III. Results of Performance Evaluation

The detector performance in relation to its efficiency at detecting $^{90}$Sr is evaluated by measuring the absolute efficiency for each radionuclide, uniformity, and the response linearity. Furthermore, the limit for detecting $^{90}$Sr is estimated by using these results. In this section, the radioactivity of the sources, the measurement setup, and a method for calculating the detection limit are described in detail. A comparison of the measured results for the four logics and the determination of the detector's effective area are also discussed.

### A. Radioactivity of the Sources

Radioactive sources of $^{90}$Sr, $^{137}$Cs (purchase from Japan Radioisotope Association), and $^{40}$K (described below) were used in this test. The radioactivities of the $^{90}$Sr and $^{137}$Cs are calculated using

$$A(t) = A_0 exp\left(-\frac{t}{\tau} ln2\right), \tag{7}$$

where $A_0 = 37$ kBq ($\pm 20\%$) is the initial radioactivity measured by the Japan Radioisotope Association, $t$ is the number of years since the previous calibration, and $\tau$ is the physical half-life. The radioactivity intensities of ten $^{90}$Sr sources and one $^{137}$Cs source were found to be $23.6 \pm 0.3$ (stat) $\pm 4.7$ (sys) kBq and $26.0 \pm 5.2$ (sys) kBq, respectively. The statistical and systematic errors were determined from the standard deviation of each radioactivity and the uncertainly in the previous calibration, respectively. Because $^{40}$K sources are not available commercially, pure potassium chloride (KCl) was used as the $^{40}$K source. The KCl source had a stable mass of $30.0 \pm 0.1$ g ($498 \pm 2$ (sys) Bq) and a radioactivity concentration of 16.6 Bq/g from $^{40}$K. It was obtained from Hayashi Pure Chemical Ind., Ltd. with a purity of 99.5% or more, and was used in the evaluation tests.

### B. Absolute Efficiency

The background rates ($N_{BG}$) for the logic of Eqs. (3)–(6) in one hour were measured to be $392 \pm 25$, $125 \pm 12$, $28795 \pm 131$, and $2297 \pm 50$ h$^{-1}$, respectively, where each error represents the standard deviation of 14 measurements. For a source placed under the center of the trigger counter, the absolute efficiency is defined as

$$\eta_x = (N_x - N_{\mathrm{BG}})/A_x T, \tag{8}$$

where $x = ^{90}$Sr, $^{137}$Cs, $^{40}$K denotes the radionuclide used, $T = 3600$ s is measurement time, and $N$ is the count rate in an hour. Results for the logic of Eq. (4) are described here. The other results are listed in Table I (discussed later). With the $^{90}$Sr source was set under the center of the trigger counter, the count rate is observed to be $147545 \pm 369$ h$^{-1}$. This corresponds to an efficiency of $[1.79 \pm 0.04\ (\mathrm{stat}) \pm 0.37\ (\mathrm{sys})] \times 10^{-3}$ Bq$^{-1}$ s$^{-1}$, where the errors of $N_{\mathrm{Sr}}$ and $N_{\mathrm{BG}}$ were dominate the statistical error, whereas the systematic error originates from the uncertainly of $A_{\mathrm{Sr}}$. For the $^{137}$Cs and $^{40}$K sources, the efficiencies are $[1.32 \pm 0.19\ (\mathrm{stat}) \pm 0.26\ (\mathrm{sys})] \times 10^{-6}$ and $[5.77 \pm 7.82\ (\mathrm{stat}) \pm 0.02\ (\mathrm{sys})] \times 10^{-6}$ Bq$^{-1}$ s$^{-1}$, respectively. As a result, the efficiency ratios, $\eta_{\mathrm{Sr}}/\eta_{\mathrm{Cs}}$ and $\eta_{\mathrm{Sr}}/\eta_{\mathrm{K}}$, were calculated to be 1,398 and 321, respectively. Therefore, the detector is effective at identifying beta rays from $^{90}$Y in the presence of other radiation.

### C. Response Linearity

A relationship between the radioactivity of $^{90}$Sr and the count rate was measured as the response linearity by setting the $^{90}$Sr sources under the trigger counter. Each 10-min count rate was measured for one additional source. The result for the logic of Eq. (4) is shown in Fig. 5. The relationship is clearly linear, with a fitted slope of $(1.74 \pm 0.06) \times 10^{-3}$ Bq$^{-1}$s$^{-1}$ and $\chi^2 = 2.6$. Therefore, the detector can measure the $^{90}$Sr radioactivity up to 250 kBq by measuring the count rate.

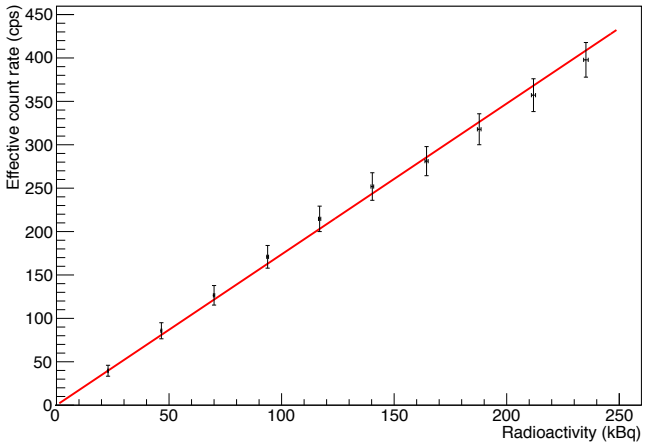


Fig. 5. Response linearity for the logic of Eq. (4). The black dots and the red solid line represent the data and the fitted linear function, respectively. The slope of the linear function is $(1.74 \pm 0.06) \times 10^{-3}$ Bq$^{-1}$s$^{-1}$ by fitting at $\chi^2 = 2.6$.

### D. Comparison of the Logics

The measured background rates, the efficiency for each radionuclide, and the efficiency ratios for the four logics are listed in Table I. Comparing Eqs. (3) and (4), the determination of $M_{th}$ (i.e., one or two) in order to measure the radioactivity concentration of $^{90}$Sr effectively is discussed here. The absolute efficiency for $^{90}$Sr in $M_{th} = 2$ is approximately 0.39 times higher than that in $M_{th} = 1$. The efficiencies for $^{137}$Cs and $^{40}$K in $M_{th} = 2$ are approximately 0.08 and 0.07 times higher than that in $M_{th} = 1$, respectively. Thus, the efficiency ratios, $\eta_{\mathrm{Sr}}/\eta_{\mathrm{Cs}}$ and $\eta_{\mathrm{Sr}}/\eta_{\mathrm{K}}$, in $M_{th} = 2$ are approximately 4.8 and 2.7 times higher than those in $M_{th} = 1$, respectively. It is more important to suppress any accidental noise for the measurement of the radioactivity concentration of $^{90}$Sr in the detector. Therefore, the logic of Eq. (4), $M_{th} = 2$, is used for the measurements.

The ratio of $\eta_{\mathrm{Sr}}$ in the logic of Eq. (4) to $\eta_{\mathrm{Sr}}$ in the logic of Eq. (5) represents the detection efficiency of the Cherenkov counter using the silica aerogel and the WLSFs for $^{90}$Sr with $M_{th} = 2$, which is estimated to be $(7.27 \pm 0.16) \times 10^{-3}$.

Furthermore, the misidentifications in $^{137}$Cs and $^{40}$K are estimated to be $(1.96 \pm 0.28) \times 10^{-5}$ and $(4.65 \pm 6.31) \times 10^{-5}$, respectively. Subtracting $N_{\rm BG}$ in the logic of Eq. (6) from $N_{\rm BG}$ in the logic of Eq. (4) gives the count rate of cosmic muons in the detector, which is estimated to be $2172 \pm 62$ h$^{-1}$. This count rate depends on the effective area of the trigger counter (30 cm $\times$ 10 cm); the count rate per unit area is estimated to be $(2.01 \pm 0.06) \times 10^{-3}$ s$^{-1}$ cm$^{-2}$. According to the known intensity of cosmic muons and a detection efficiency of 99% or more in the veto counter, the detection efficiency for the cosmic muons in the Cherenkov counter with $M_{th} = 2$ is estimated to be $(4.57 \pm 0.14) \times 10^{-2}$. The ratio of the detection efficiency for $^{90}$Sr to the efficiency for cosmic muons is approximately 16%, which is consistent with the percentage (13.4%) of the beta rays with 1.31–2.28 MeV in the beta rays emitted from the radiation equilibrium conditions of $^{90}$Sr and $^{90}$Y. Thus, it is demonstrated that the beta rays with energies of 1.31–2.28 MeV from $^{90}$Y are detected by the Cherenkov counter.

TABLE I
MEASURED BACKGROUND RATE, THE ABSOLUTE EFFICIENCY, AND THE EFFICIENCY RATIOS ON THE RADIONUCLIDES IN EACH LOGIC

| | |
|---|---|
| Logic (3): $Trigger \cap \overline{VETO} \cap AC(M \geq 1)$ | |
| $N_{\rm BG}$ | $392 \pm 25$ h$^{-1}$ |
| $\eta_{\rm Sr}$ | $[4.58 \pm 0.09\ (\text{stat}) \pm 0.94\ (\text{sys})] \times 10^{-3}$ Bq$^{-1}$ s$^{-1}$ |
| $\eta_{\rm Cs}$ | $[1.61 \pm 0.06\ (\text{stat}) \pm 0.32\ (\text{sys})] \times 10^{-5}$ Bq$^{-1}$ s$^{-1}$ |
| $\eta_{\rm K}$ | $[4.07 \pm 1.38\ (\text{stat}) \pm 0.02\ (\text{sys})] \times 10^{-5}$ Bq$^{-1}$ s$^{-1}$ |
| $\eta_{\rm Sr}/\eta_{\rm Cs}$ | 285 |
| $\eta_{\rm Sr}/\eta_{\rm K}$ | 113 |
| Logic (4): $Trigger \cap \overline{VETO} \cap AC(M \geq 2)$ | |
| $N_{\rm BG}$ | $125 \pm 12$ h$^{-1}$ |
| $\eta_{\rm Sr}$ | $[1.79 \pm 0.04\ (\text{stat}) \pm 0.36\ (\text{sys})] \times 10^{-3}$ Bq$^{-1}$ s$^{-1}$ |
| $\eta_{\rm Cs}$ | $[1.32 \pm 0.19\ (\text{stat}) \pm 0.26\ (\text{sys})] \times 10^{-6}$ Bq$^{-1}$ s$^{-1}$ |
| $\eta_{\rm K}$ | $[5.77 \pm 7.83\ (\text{stat}) \pm 0.02\ (\text{sys})] \times 10^{-6}$ Bq$^{-1}$ s$^{-1}$ |
| $\eta_{\rm Sr}/\eta_{\rm Cs}$ | 1,352 |
| $\eta_{\rm Sr}/\eta_{\rm K}$ | 310 |
| Logic (5): $Trigger \cap \overline{VETO}$ | |
| $N_{\rm BG}$ | $28795 \pm 131$ h$^{-1}$ |
| $\eta_{\rm Sr}$ | $[2.47 \pm 0.01\ (\text{stat}) \pm 0.51\ (\text{sys})] \times 10^{-1}$ Bq$^{-1}$ s$^{-1}$ |
| $\eta_{\rm Cs}$ | $[6.75 \pm 0.01\ (\text{stat}) \pm 0.14\ (\text{sys})] \times 10^{-2}$ Bq$^{-1}$ s$^{-1}$ |
| $\eta_{\rm K}$ | $[1.24 \pm 0.01\ (\text{stat}) \pm 0.01\ (\text{sys})] \times 10^{-1}$ Bq$^{-1}$ s$^{-1}$ |
| $\eta_{\rm Sr}/\eta_{\rm Cs}$ | 3.67 |
| $\eta_{\rm Sr}/\eta_{\rm K}$ | 2.00 |
| Logic (6): $Trigger \cap AC(M \geq 2)$ | |
| $N_{\rm BG}$ | $2297 \pm 50$ h$^{-1}$ |
| $\eta_{\rm Sr}$ | $[1.80 \pm 0.05\ (\text{stat}) \pm 0.37\ (\text{sys})] \times 10^{-3}$ Bq$^{-1}$ s$^{-1}$ |
| $\eta_{\rm Cs}$ | $[2.30 \pm 0.49\ (\text{stat}) \pm 0.46\ (\text{sys})] \times 10^{-6}$ Bq$^{-1}$ s$^{-1}$ |
| $\eta_{\rm K}$ | $[1.57 \pm 2.58\ (\text{stat}) \pm 0.01\ (\text{sys})] \times 10^{-5}$ Bq$^{-1}$ s$^{-1}$ |
| $\eta_{\rm Sr}/\eta_{\rm Cs}$ | 800 |
| $\eta_{\rm Sr}/\eta_{\rm K}$ | 114 |

### *E. Uniformity of the Efficiency with Source Position*

The uniformity of the efficiency was measured by setting the $^{90}$Sr source at 75 points under the trigger counter with an entrance of 300 mm $\times$ 100 mm., and measuring for 600 s at each point. The uniformity of the logic of Eq. (4) is shown in Fig. 6. The efficiency for $^{90}$Sr tends to peak at the center and falls away at the edges. Because the beta rays are emitted isotropically from the source, fewer particles pass through the entrance at the edges than do so at the center. As a result, the mean efficiency is $(1.11 \pm 0.53) \times 10^{-3}$ Bq$^{-1}$s$^{-1}$. The dashed line in Fig. 6 represents the area of 200 mm $\times$ 40 mm of best efficiency, in which the mean efficiency is $(1.75 \pm 0.38) \times 10^{-3}$ Bq$^{-1}$s$^{-1}$.

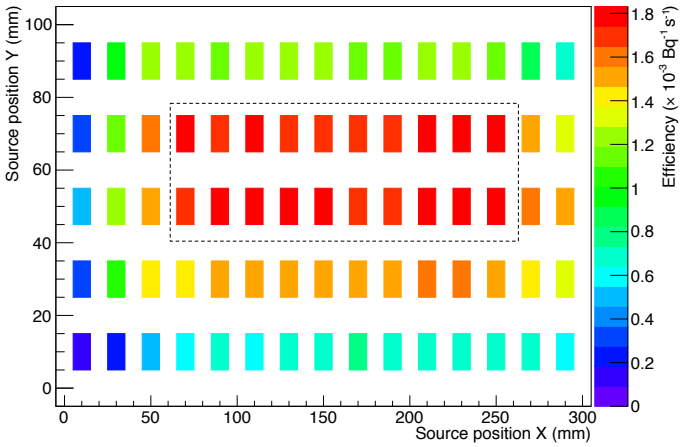


Fig. 6. Uniformity of efficiency with source position with the logic of Eq. (4). The $^{90}$Sr source was placed at 75 points (X and Y) under the trigger counter. The dashed line represents the area of best efficiency.

### *F. Detection Limit of* $^{90}$Sr

The detection limit of $^{90}$Sr was estimated by considering that a sample that also contained $^{137}$Cs and $^{40}$K. This is because the must be able to inspect samples with relatively low concentrations of $^{90}$Sr in radiation environment. Here the radioactivity concentration of $^{137}$Cs is taken as $A'_{\rm Cs} = 100$ Bq kg$^{-1}$ (concentration limit set by the Japanese Government). The radioactivity concentration of $^{40}$K in seawater (seafood) samples is taken as $A'_{\rm K} = 12.1\ (135)$ Bq kg$^{-1}$. This was determined from an average of potassium concentration of 0.39 g L$^{-1}$ in seawater [16] and a concentration of 4.44 g kg$^{-1}$ in raw tuna [17]. To expose radioactivity inside the sample, the sample volume should be compress by drying or heating; the compression factor for seawater (seafood) is $\varepsilon = 0.3\ (0.01)$ because seawater and seafood contain approximately 70% and 99% or more pure water, respectively. The dried-sample weight ($m$), with a density of 1 g cm$^{-3}$, depends on the detector's effective area because the sample paste thickness is approximately 1 mm. If the effective area is taken to be the whole entrance window, the measurements yield $m = 30$ g and $\eta_{\rm Sr} = 1.11 \pm 0.53$ kBq$^{-1}$ s$^{-1}$. If the effective area is taken to be the area of best efficiency, the measurements yield $m = 8$ g. The determination of the effective area is important to optimize the detection limit of $^{90}$Sr, as discussed below. Here, the former set of parameters us assumed. When the sample is placed under the trigger counter, the count rate per an hour ($N$) is

$$N = (\eta_{\rm Sr} A'_{\rm Sr} + \eta_{\rm Cs} A'_{\rm Cs} + \eta_{\rm K} A'_{\rm K}) m \varepsilon^{-1} T + N_{BG}, \qquad (9)$$

where $A'_{\rm Sr}$ is the radioactivity concentration of $^{90}$Sr and $T$ is measuring time of 3600 s. The background count rate ($N'_{BG}$) when the sample contains no $^{90}$Sr is

$$N'_{BG} = (\eta_{\rm Cs} A'_{\rm Cs} + \eta_{\rm K} A'_{\rm K}) m \varepsilon^{-1} T + N_{BG}. \qquad (10)$$

The detection limit of $^{90}$Sr radioactivity ($A_{\rm Sr}^{\rm min}$) is

$$A_{\rm Sr}^{\rm min} = \frac{3\sqrt{N_{\rm BG} + (\eta_{\rm Cs}A'_{\rm Cs} + \eta_{\rm K}A'_{\rm K})m\varepsilon^{-1}T}}{\eta_{\rm Sr}m\varepsilon^{-1}T}, \qquad (11)$$

which comes from the minimum of $A_{\rm Sr}$ satisfying a condition in Kaise's theorem, namely $N > N'_{\rm BG} + 3\sqrt{N'_{\rm BG}}$ [18]. As a result, the detection limit is estimated to be $2.75 \pm 1.27$ (seawater) and $81.8 \pm 38.0$ Bq kg$^{-1}$ (seafood). The latter determination result is listed in Table II.

TABLE II
DETECTION LIMIT OF $^{90}$Sr IN WHICH TWO CASES OF THE DETERMINATION OF THE EFFECTIVE AREA

| | The entrance window | The area of best efficiency |
|---|---|---|
| The effective area | 300 mm × 100 mm | 200 mm × 40 mm |
| The sample weight | 30 g | 8 g |
| $\eta_{Sr}$/kBq$^{-1}$s$^{-1}$ | $1.11 \pm 0.53$ | $1.75 \pm 0.38$ |
| $A_{\rm Sr}^{\rm min}$(seawater) | $2.75 \pm 1.27$ Bq kg$^{-1}$ | $6.83 \pm 0.15$ Bq kg$^{-1}$ |
| $A_{\rm Sr}^{\rm min}$(seafood) | $81.8 \pm 38.0$ Bq kg$^{-1}$ | $204 \pm 4$ Bq kg$^{-1}$ |

### G. Determination of the Effective Area

According to Eq. (11), the detection limit depends on the efficiency of $^{90}$Sr, the effective area contributed by the sample weight, the background rate, and the measuring time. It is necessary to determine the size of the effective area in order to measure the concentration of $^{90}$Sr in the sample effectively. In this discussion, it is assumed that the sample has a uniform concentration of $^{90}$Sr. Two types of the detection limit of $^{90}$Sr are estimated, as listed in Table II: the mean efficiency over 300 mm × 100 mm, and the best efficiency inside the dashed line (see Fig. 6). In the former case, the detection limits $A_{\rm Sr}^{\rm min}$(seawater) and $A_{\rm Sr}^{\rm min}$(seafood) with the logic of Eq. (4) are $2.75 \pm 1.27$ and $81.8 \pm 38.0$ Bq kg$^{-1}$, respectively. In the latter case, the detection limits are $6.83 \pm 0.15$ and $204 \pm 4$ Bq kg$^{-1}$. Clearly, the former case is better than the latter; thus, the effective area is taken as 300 mm × 100 mm.

## IV. Conclusion

A new detector—a real-time $^{90}$Sr counter—was developed based on a threshold-type Cherenkov detector using the silica aerogel. Its purpose is to aid the recovery of the fisheries in Fukushima Prefecture, Japan, for which adequate sensitivity to beta rays from $^{90}$Y and lower sensitivity to other radiation (e.g., $^{137}$Cs and $^{40}$K). A veto counter was used to cover the trigger and the Cherenkov counters, and could suppress events associated with cosmic-ray muons coming arriving with zenith angles of 0–90°. The test sample must be dried and made into a paste without chemical extraction. From performance tests using calibrated sources, the $^{90}$Sr efficiency was evaluated to be $[1.79 \pm 0.04\ (\rm stat) \pm 0.36\ (\rm sys)] \times 10^{-3}$ Bq$^{-1}$ sec$^{-1}$ at the center of an effective area of 300 mm × 100 mm. The efficiency ratios of $^{90}$Sr to $^{137}$Cs and $^{40}$K were estimated to be 1,352 and 310, respectively. The radioactivity concentration of $^{90}$Sr in seawater or seafood samples could be measured based on the count rate in the environmental radiation background. The detection limit of $^{90}$Sr concentration was estimated to be $2.7 \pm 1.3$ (seawater) and $82 \pm 38$ Bq kg$^{-1}$ (seafood) in a measuring time of one hour.

## Appendix

To be able to understand this study in more detail, the following properties of nuclides are listed in Table III: physical half-life ($\tau_{\rm phys}$), maximum kinetic energy of a beta ray ($K_{\rm max}$), energy of a gamma ray ($E_\gamma$), decay channels, and branching ratio ($\Gamma$). Caesium-137 has two decay channels with a physical half-life of 30.2 yr. In the decay channel of $^{137}{\rm Cs} \rightarrow {}^{137{\rm m}}{\rm Ba} \rightarrow {}^{137}{\rm Ba}$, after a beta ray of $K_{\rm max} = 0.512$ MeV is emitted when $^{137}$Cs decay to $^{137{\rm m}}$Ba in 94.6%, the $^{137{\rm m}}$Ba decays to stable $^{137}$Ba and emits a gamma ray of $E_\gamma = 0.662$ MeV. Alternatively, $^{137}$Cs can decay to $^{137}$Ba directly and emit a beta ray of $K_{\rm max} = 1.174$ MeV in 5.4%. Strontium-90 has a physical half-life of 28.8 yr, decays to $^{90}$Y, and emits a beta ray of $K_{\rm max} = 0.546$ MeV. Yttrium-90 has a physical half-life of 64 h, decays to stable $^{90}$Zr, and emits a beta ray of $K_{\rm max} = 2.28$ MeV. Strontium-90 and its daughter ($^{90}$Y) reach radioactive equilibrium. Caesium-137 and $^{90}$Sr are artifact radionuclides produced by nuclear fission and are water soluble. In nature, 0.0117% of environmental potassium is $^{40}$K. The radiation dose has been estimated as 0.18 mSv yr$^{-1}$ by internal exposures of approximately 60 Bq kg$^{-1}$. Potassium-40 has a physical half-life of $1.25 \times 10^9$ yr and emits a beta ray of $K_{\rm max} = 1.31$ MeV if it decays to $^{40}$Ca (89.1%) or a gamma ray of $E_\gamma = 1.461$ MeV if it decays to $^{40}$Ar (10.7%).

TABLE III
PROPERTIES OF RADIONUCLIDES

| Decay channel ($\tau_{\rm phys}$) | $K_{\rm max}$ | $E_\gamma$ | $\Gamma$ |
|---|---|---|---|
| $^{90}{\rm Sr} \rightarrow {}^{90}{\rm Y}$ (28.8 years) | 0.546 MeV | | 100% |
| $^{90}{\rm Y} \rightarrow {}^{90}{\rm Zr}$ (64 hours) | 2.280 MeV | | 100% |
| $^{137}{\rm Cs} \rightarrow {}^{137{\rm m}}{\rm Ba} \rightarrow {}^{137}{\rm Ba}$ | 0.512 MeV | 0.662 MeV | 94.6% |
| $^{137}{\rm Cs} \rightarrow {}^{137}{\rm Ba}$ (30.2 years) | 1.174 MeV | | 5.4% |
| $^{40}{\rm K} \rightarrow {}^{40}{\rm Ca}$ | 1.311 MeV | | 89.3% |
| $^{40}{\rm K} \rightarrow {}^{40}{\rm Ar}$ ($1.25 \times 10^9$ years) | | 1.461 MeV | 10.7% |

## References


[1] G. Katata, H. Terada, H. Nagai, and M. Chino, " Numerical reconstruction of high dose rate zones due to the Fukushima Dai-ichi Nuclear Power Plant accident", J. Environ. Radio., vol. 111, pp. 2-12, 2012.

[2] K. Shozugawa, N. Nogawa, and M. Matsuo, " Deposition of fission and activation products after the Fukushima Dai-ichi nuclear power plant accident", Environ. Pollution, vol. 163, pp. 243-247, 2012.

[3] ICRP," Age-dependence Doses to Members of the Public from Intake of Radionuclides: Part 4 Inhalation Dose Coefficients", ICRP publication 71, 1995.

[4] S. Yamasaki, J. Imoto, G. Furuki, A. Ochiai, T. Ohnuki, K. Sueki, K. Nanba, R. C. Ewing, and S. Utsunomiya, " Radioactive Cs in the estuary sediments near Fukushima Daiichi Nuclear Power Plant", Scien. Total Environ., vol. 551-552, pp. 155-162, 2016.

[5] J. Tsuboi, S. Abe, K. Fujimoto, H. Kaeriyama, D. Ambe, K. Matsuda, M. Enomoto, A. Tomiya, T. Morita, T. Ono, S. Yamamoto, and K. Iguchi, " Exposure of a herbivorous fish to $^{134}$Cs and $^{137}$Cs from the riverbed following the Fukushima disaster", J. Environ. Radio., vol. 141, pp. 32-37, 2015.

[6] H. Nabeshi, T. Tsutsumi, and Y. Uekusa, A. Hachisuka, R. Matsuda and R. Teshima," Surveillance of Strontium-90 in Foods after the Fukushima Daiichi Nuclear Power Plant Accident", Food Hygi. Safe. Science, vol. 56, no. 4, pp. 133-143, 2015.

[7] C. Testa, D. Desideri, F. Guerra, M. A. Meli, C. Roselli, and G. Jia, “ The importance of separation chemistry for the determination of radionuclides in environmental samples”, J. Radio. Nucl. Chem., vol. 229, Issue 1, pp. 23-32, 1998.
[8] H. Ito, S. Han, A. Kobayashi, N. Kaneko, H. Kawai and M. Tabata, “ Identification of $^{90}\mathrm{Sr}/^{40}\mathrm{K}$ based on Cherenkov detector for recovery from the Fukushima nuclear accident”, JPS Conf. Proc., 070002, 2016.
[9] S. Ijima, S. Han, H. Ito, H. Kawai, S. Kodama, and D. Kumogoshi, “ Development of Realtime 90Sr Counter Used in Low Rate Radioactive”, in: 2014 IEEE NSS/MIC, N09-40, 2014.
[10] S. Iijima, H. Ito, D. Kumogoshi, K. Satoshi, H. Kawai, M. Tabata, K. Mase, and H. Nakayama, “ Development of Realtime 90Sr Counter”, in: 2013 IEEE NSS/MIC, NPO1-169, 2013.
[11] R. Pestotnik, S. Korpar, P. Krizăn, and R. Dolenec, “ Cherenkov detector of 90Sr based on aerogel as radiator”, Nucl. Instrum. Methods A, vol. 595, Issue 1, pp. 278-280, 2008.
[12] M. Tabata, I. Adachi, H. Kawai, T. Sumiyoshi, and H. Yokogawa, “ Hydrophobic silica aerogel production at KEK ”, Nucl. Instrum. Methods A, vol. 668, pp. 64-70, 2012.
[13] Kuraray Co. Ltd., data sheet, Available: http://kuraraypsf.jp.
[14] Hamamatsu Photonics K.K., data sheet, Available: http://www.hamamatsu.com.
[15] Bee Beans Technologies Co., Ltd., data sheet, Available: https://www.bbtech.co.jp.
[16] Keith E. Chave, “ Chemical reactions and the composition of sea water ”, J. Chem. Educ., vol. 48, Issue 3, pp. 148-151, 1971.
[17] Mark Roe, Susan Church, Hannah Pinchen, Paul Finglas, “ Nutrient Analysis of Fish and Fish Products: Analytical Report ”, Publication of Department of Health, GOV. UK, 2013.
[18] H. Kaiser, “ Zum Problem der Nachweisgrenze ”, Fresenius Z. Anal. Chem., vol. 209, Issue 1, pp. 1-18, 1965.